Numerical Prediction of Flow Recirculation Length Zone in an Artery with Double Stenosis at Low and High Reynolds Numbers

O. T. Olakoyejo[1*] , G.A Hammond[1], O. O. Adewumi[1], Sogo Abolarin[2] , A.O Adelaja [1], A. I. Fetuga[1] , A.S. Shote[3] , S.A. Aasa[3,4]

[1]Department of Mechanical Engineering, University of Lagos, Nigeria
[2]Department Engineering Sciences, University of the Free State, Bloemfontein, South Africa
[3]Department of Mechanical Engineering Olabisi Onabanjo University,
[4]Department of Mechanical and Aeronautical Engineering, University of Pretoria, South Africa
[*]Email: *oolakoyejo@unilag.edu.ng*

Abstract
This work presents simulation of arterial stenosis utilizing ANSYS (Fluent) Computational Fluid Dynamics (CFD) software package for better understanding of blood flow dynamics and to estimate the risk of complication. The aim of the paper is to investigate and study the effects of low and high Reynold's number on recirculation zone length in arteries with varying levels of double stenosis. Blood flow was numerically simulated to predict the recirculation zone length and wall shear stress. An artery with double stenosis was studied and for the purpose of this investigation, stenosis levels of 15/15%, 75/75%, 15/75%, 75/15%, 15/60%, 20/60%, 45/60% 60/60%, and 75/60% in terms of proximal and distal stenosis are studied over the Reynolds number ranging from 150 to 3000. Blood was a Newtonian fluid flowing as a steady, three-dimensional, incompressible fluid. The velocity flow streamlines, and wall shear stress contours are presented. Results revealed that when varying both distal and proximal stenosis, as Reynolds number increases, recirculation zone length decreases in lower levels of stenosis between 15/60% and 45/60% while it remains relatively constant for higher levels of stenosis 60/60% and 75/60%. It was also revealed that when varying both distal and proximal stenosis, as Reynolds number increases, maximum wall shear stress increases gradually at lower levels of stenosis with almost equal values. At higher levels of stenosis, there was rapid increase in maximum wall shear stress as Reynolds number increases.

Keywords: Numerical simulation, double stenosis, distal stenosis, proximal stenosis, recirculation zone length, wall shear stress.

Nomenclature

Symbols	Description	Unit
Z	axial direction	rad
Θ	circumferential direction	rad
ρ	density of blood	kg/m^3
Y_ω	destruction term	J
Y_k	destruction term	J
μ	dynamic viscosity	kg/m.s
$\Gamma_k \wedge \Gamma_\omega$	effective diffusivity	m^2/s
G_k , G_ω	generation terms	J/m^3
P	Pressure	N/m^2
r	radial direction	m
ω	specific dissipation rate	m^2/s^3
S_{ij}	Strain-rate tensor	s^{-1}
k	turbulence kinetic energy	m^2/s^2

1.0 INTRODUCTION

In the last few years, cardiovascular diseases (CVD) have become the most common cause of death across the globe, with a total of 18million deaths, according to Dattani *et al.* (2021). In recent times, some lifestyle factors that individuals engage in have contributed to the development of obstructed arteries, some of which are smoking, high blood cholesterol levels,

and potentially genetic predisposition (Koosha *et al..,* 2024). Stenosis is a kind of cardiovascular disease (CVD) that involves the accumulation of plaque on the artery's inner wall, this leads to artery narrowing and unusual blood flow patterns. Plaques are substances made up of cholesterol and fat, that are found in unhealthy foods like bacon, sausages, French fries, etc (Mount Sinai, 2024). Formation of plague in blood vessels is one of the major causes of reduction in blood flow in arteries, which results in minimized transfer of blood to different human organs. The segment of the blood vessel where the stenosis is located generates a high pressure, resulting in an increase in velocity around that region. Over the years, several experimental and numerical studies have been carried out to study the effects of stenosis on haemodynamic indicators.

Mojra *et al.* (2007) carried out computational study of asymmetric arterial stenosis with an application of fluid-solid interaction. The study reviewed simulations of plaque severity and analyzed the eccentricity impacts of atherosclerotic carotid arteries with stenoses that are asymmetric on haemodynamic parameters in models. The findings of the simulation showed that the increase in severity of stenosis will lead to a non-linear increase in pressure at the inlet and becomes critical at a severity level of 78% when the pressure at the upstream rises to about 100 mmHg.

Alshare *et al.* (2013) performed simulations of steady blood flow in an axisymmetric artery with multi-stenoses that are exposed to a static magnetic field with an assumption of a laminar flow. The study aimed at examining the effects of size of artery, strength of magnetic field, and non-Newtonian blood behavior on the wall shear stress of the artery as well as pressure drop around the stenotic zone. It was discovered that wall shear stress and pressure drop increases as artery size decreases.

Meanwhile, Doutel *et al.* (2018) introduced a new method called the diffusional method, to create three-dimensional models of irregular stenotic arteries. They carried out a computational study that used a simple and efficient method to create an irregular stenotic artery for numerical and in vitro hemodynamic studies. This method deduced the part of the artery that is susceptible to stenoses by identifying regions with having minimal wall shear stress.

Alshare *et al.* (2015) decided to carry the research further by considering multiple stenosis. They carried out simulations using ANSYS Fluent considering blood as a non-Newtonian fluid flowing in a pulsatile manner in an artery with axisymmetric multi-stenosis. The artery is exposed to a static magnetic field. The effects of size of artery and intensity of magnetic field on transient wall shear stress, mean shear stress, and pressure reduction were reviewed on healthy, diabetic and anemic blood. It was discovered that there will be a 15% pressure drop if the magnetic field is raised.

Dwidmuthe *et al.* (2015) took a different approach and developed a quantitative relationship that permits easy analysis of flow dynamics in arterial stenosis by examining wall shear stress using CFD and Response Surface Methodology. Different stenosis severity levels were studied: 10%, 25%, 50%, 75%, 90%. Dimensionless parameter, D/Ls which represents the diameter of artery/length of stenosis was also considered and the values varied from 0.2, 0.3, 0.4, 0.5, to 0.6. To evaluate the influence of these factors, pressure drop and Wall Shear Stress across the stenotic zones were analyzed as response variables.

Putting nanoparticles into consideration, Fetuga *et al.* (2023) also carried out a computational study of blood flowing through an artery that is affected by both aneurysm and stenosis in the presence of metallic nanoparticles as well as non-metallic nanoparticles suspended in blood. The effects of various nanoparticles such as Aluminum Oxide, Copper (II) oxide, Silicon dioxide as well as Zinc oxide, the concentration of all these with varying diameters on blood flow

parameters (velocity distribution, temperature distribution, Nusselt number, skin friction coefficient, etc.) was studied. The results showed that the velocity of blood flow was highly decreased when a 4.0% concentration of Copper (II) oxide was used, as opposed to other nanoparticles.

Carvalho *et al.* (2020) analyzed and compared numerically using CFD, the behaviour of blood flow, with the application of the k-w SST model and the assumption of laminar flow. Study of the impacts of Newtonian and non-Newtonian models was also carried out.

Shaikh *et al.* (2023) studied the characteristics of blood flowing through an artery that has been affected by a single stenosis as well as multiple stenoses. A thorough analysis was carried out on flow patterns and results showed a change in blood flow pattern from laminar to turbulent for 30% and 50% level of stenosis for single stenosis and 30% level for multiple stenosis. The results showed that blood flow is laminar in 30% stenotic level for single stenosis. The study also predicted the excess pressure reduction over the stenotic zone and the rise in the velocity is noticed at the middle of the artery.

In an in-depth study that was carried out by Nadeem *et al.* (2023), blood was simulated as a non-Newtonian fluid in an idealized stenotic artery. Proper examination was done on 50%-80% levels of stenosis in the arteries in area reduction. For a 50–70% level of the stenosis, the lowest pressure was noticed in Newtonian fluid, and the maximum pressure was recorded in Casson, while Quemada lied in between them. It was also discovered that pressure drop around the stenotic zone is more significant.

Koosha *et al.* (2023) explored the role of hybrid nanofluids by studying its impact on transfer of heat and pulsatile flow of Newtonian blood through 3D occluded artery. The nanoparticles utilized for the nanofluid were silver and gold. The aim of the study was to study the effects of pulsating velocity of blood on transfer of heat within biological systems, focusing on blood flow in stenotic arteries. Zhao *et al.* (2023) carried out time-resolved simulation of blood flow through descending coronary artery located at the left anterior. They investigated the influence of varying level of stenosis on the haemodynamic features in descending coronary artery located at the left anterior. There was no significant change in haemodynamic parameters in the cases where stenosis level was less than 50% while there were sudden and notable changes in haemodynamics when the level of stenosis rose from 60 to 70%. When the level of stenosis rose beyond 70%, a significant difference in pressure, WSS, and blood flow velocity at the point of the stenosis was noticed. Although OSI and RRT rose as the level of stenosis increased, some abnormalities were noticed, even in mild stenosis.

In another study carried out by Kabir *et al.* (2018), numerical simulation was done with varying Reynolds numbers (Re) to study the effect of stenosis on spiral blood flow in an artery. The simulation was performed utilizing the standard k-ω model and an artery with a 75% level of single stenosis was considered. The maximum Turbulent Kinetic Energy (TKE) was found to be at the stenotic center and it increased with an increase in Reynolds number. Similarly, wall shear stress also reached its peak at the stenotic point and increased as Reynolds number increased.

Mamun *et al.* (2018) investigated blood flow behaviour in carotid arteries while taking blood as a non-Newtonian fluid. It was observed that Reynolds number increased unusually at peak systole at the region of the throat for an 85% level of stenosis in the carotid artery. According to them, a healthy artery does not have its flow disturbed at the whole cardiac cycle with an exception at early diastole. The paper revealed that the reason behind this is unsteady flow conditions. Meanwhile, a moderate flow disturbance was observed in the 65% level of stenosis in the carotid artery at the whole cardiac cycle with exception at the early systole. In the 85%

stenotic carotid artery, a very similar disturbance in the flow was noticed but it was more severe. In summary, flow disturbance increases as the level of stenosis increases.

Moawad *et al.* (2022) studied the influence of double-diffusion convection through an artery that is curved with stenosis and aneurysm. It was observed that the velocity of blood flow is improved in the presence of the electro-osmotic field. It was also noticed that the axial velocity reduced greatly as the number of Grashof nanoparticles increased while the axial velocity increased as the number of Grashof solutes and Grashof thermals increased.

Kabir *et al.* (2021) carried out another research on pulsatile transitional blood flowing through an artery with varying levels of symmetric stenosis. The study was carried out on a normal artery, arteries with single stenosis and arteries with double stenosis. It was discovered that at the stenotic region for both single and double stenosis, axial velocity increased with increasing level of stenosis (in terms of area reduction). Upon investigation on the pressure variation, it was also found that as the level of stenosis increased, the pressure reduction increased and a maximum pressure reduction of 70Pa was recorded for a 75-75% stenotic artery. Hence, the higher the stenotic level, the higher the pressure drops. Results showed that Wall Shear Stress increased with increasing level of stenosis.

Song *et al.* (2020) explored topology of flow and hemodynamics on tortuous coronary artery that have symmetrical and asymmetrical stenosis. The study showed that larger artery surface of time averaged wall shear stress below critical value is generally associated with pulse rates that are smaller, higher severity of stenosis and an increased distance between point of stenosis and tortuousity both for arteries that are curved and spiral. However, some exceptions were found in the cases of 6 mm distance in curved artery that has symmetrical stenosis and stenosis level of 50% in spiral artery.

Tabe *et al.* (2020) focused on detecting laminar-to-turbulence and re-laminarization zones for low Reynolds number turbulent flow of blood in arteries with large stenoses. In this study, the major focus was on the impact of narrowing in the field of flow in a distinctive way. The results of this study showed that the part-by-part simulation is an appropriate method for the study of arterial stenosis and can also be applied to computational simulation of narrowed tubes in various applications with low Reynolds number that can lead to a transition from laminar to turbulence and re-laminarization.

Changdar *et al.* (2015) carried out numerical simulation of non-linear pulsatile blood flow through an artery with multiple stenosis, taking blood as a Newtonian fluid. A suitable non-linear blood flow model was used to study the effect of periodic body acceleration through an artery with multiple stenosis with the help of FDM (Finite Difference Method).

Hussain *et al.* (2023) carried out numerical simulation of Newtonian blood flow of unsteady blood flow and heat transfer through stenosis of inconsistent shapes and dilatability. This contemporary research was conducted to assess the features of blood flow and level of blockage generated in the pathway of arteries of various geometries. The behaviour of blood flow was studied in a stenotic artery to determine velocity, pressure, and changes in temperature caused by this disease. It was found that the stenosis shape has a significant effect on the velocity, total pressure reduction and temperature across the arterial stenotic zone.

Kamangar *et al.* (2021) studied the impact of multiple stenoses on haemodynamics parameters in coronary artery models that were idealized with varying levels of stenosis as well as distance between the stenoses. The results revealed that the pressure reduction is maximum across the 90% stenotic level. It was also observed that the pressure reduction increased as the distance between the proximal and distal stenosis decreased for the model P70_D70 where P70 refers to a 70% level of proximal stenosis and D70 refers to a 70% level d distal stenosis. A

recirculation zone is usually formed downstream the stenosis and is obstructed by the presence of distal stenosis as the spacing between them decreases, this could lead to further development of stenosis in the areas of disturbed flow. The wall shear stress was discovered to increase with an increase in the distance between the proximal and distal stenosis across the distal stenosis. The peak of the wall shear stress was recorded at a 90% level of stenosis.
Daniel *et al.* (2023) validated an initial numerical model to determine regionalized flow of blood in coronary arteries. The three-dimensional coronary structure of 20 patients with severe coronary syndrome was reconstructed from angiograms. A pressure gradient was applied to the reconstructed geometry utilizing CFD to compute all flows. The side branch flow was modelled as a wall boundary that is porous. The magnitude of side branch flow was based on a homogeneous model with a loss of flow along the whole length of the artery; and a regionalized model that has its flow proportional to local taper.

2.0 METHODOLOGY

2.1 Geometry Description

Consider blood flowing through a double-stenotic artery with a diameter D and a Length L. Blood flowing in the positive z-axis as shown in Figure 1 and 2 below. The distal stenosis is located 4D from the inlet and 23D from the outlet. The proximal stenosis is located at 9.4D from the inlet and 17.6D from the outlet. These dimensions are sufficient for a fully developed flow to be achieved.

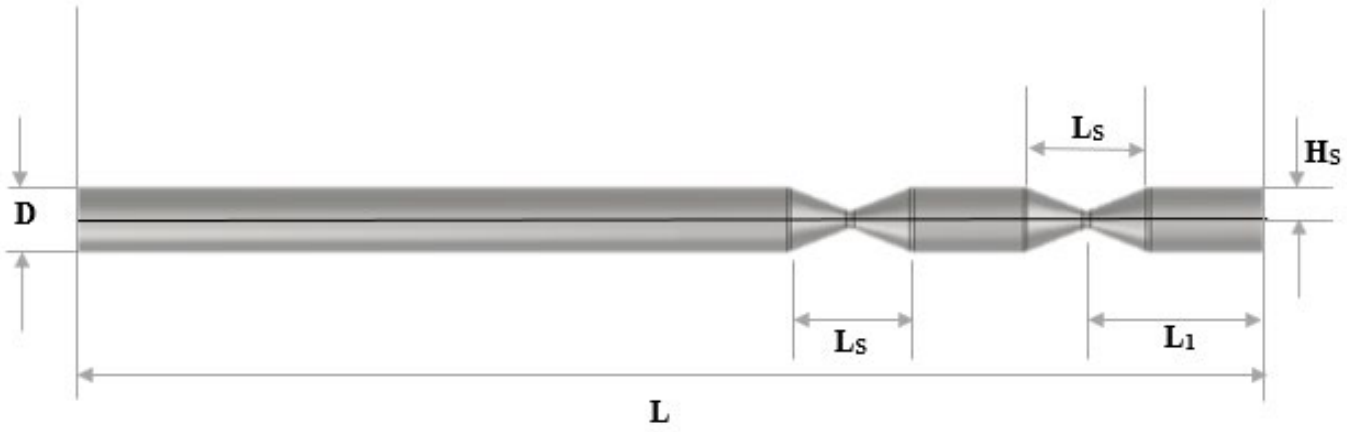

Figure 1: 2D schematic diagram of an artery with 75% double stenosis

Figure 2: 3D diagram of an artery with 75% double stenosis

2.1.1 Geometry Parameters

Table 1 shows the dimensions of the various parameters used:

Table 1: Table of geometry

Parameter	Dimension (mm)
L	27D
D	5
R	2.6D
Hs	0.075D, 0.1D, 0.15D, 0.225D, 0.3D, 0.375D
Ls	2.8D
L1	4D

2.1.2 Various Levels of Stenosis

For the purpose of this work, the following levels of stenosis are considered. All 7 geometries are created using ANSYS Design Modeler are shown in Figure 3(a)-(g).

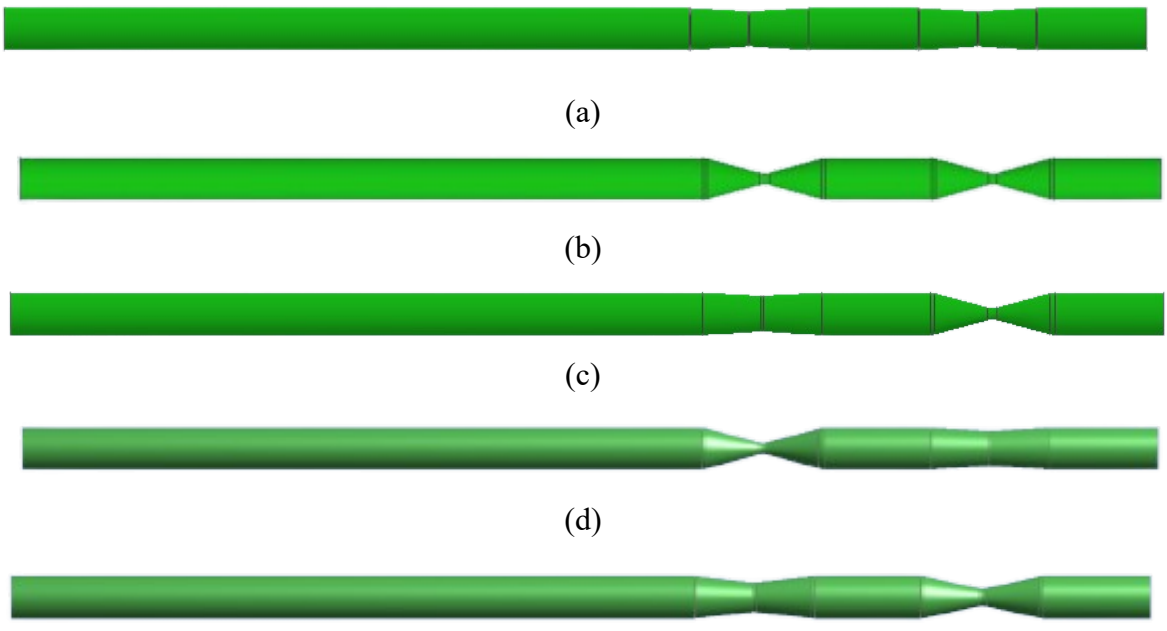

(a)

(b)

(c)

(d)

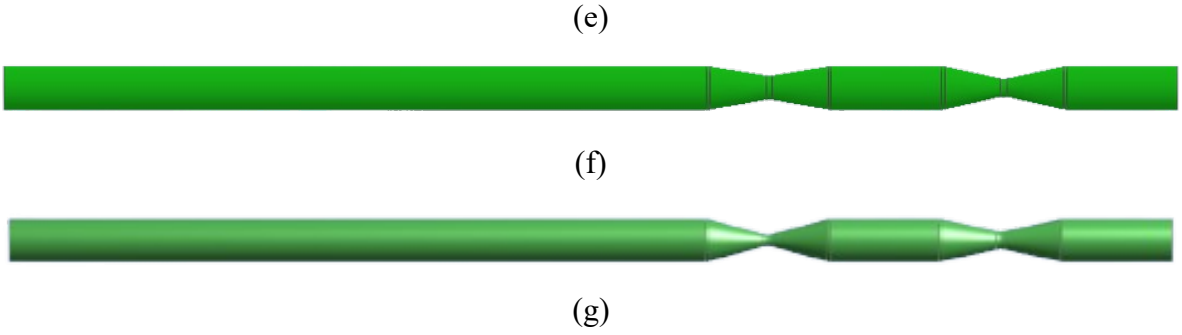

Figure 3: 2D schematic diagram of an artery with (a)15% double, (b) 75% double, (c) 15% proximal and 75% distal, (d) 75% proximal and 15%, (e) 20% proximal and 60% distal, (f) 45% proximal and 60% distal and (g) 75% proximal and 60% distal stenosis

2.2 Mesh Generation

The ANSYS Mesh is used to generate the mesh. A multizone structured meshing with hexa core is used (Figure 4 (a)-(e)). The stenotic sites and the walls are inflated with a smooth transition inflation to a maximum of five layers.

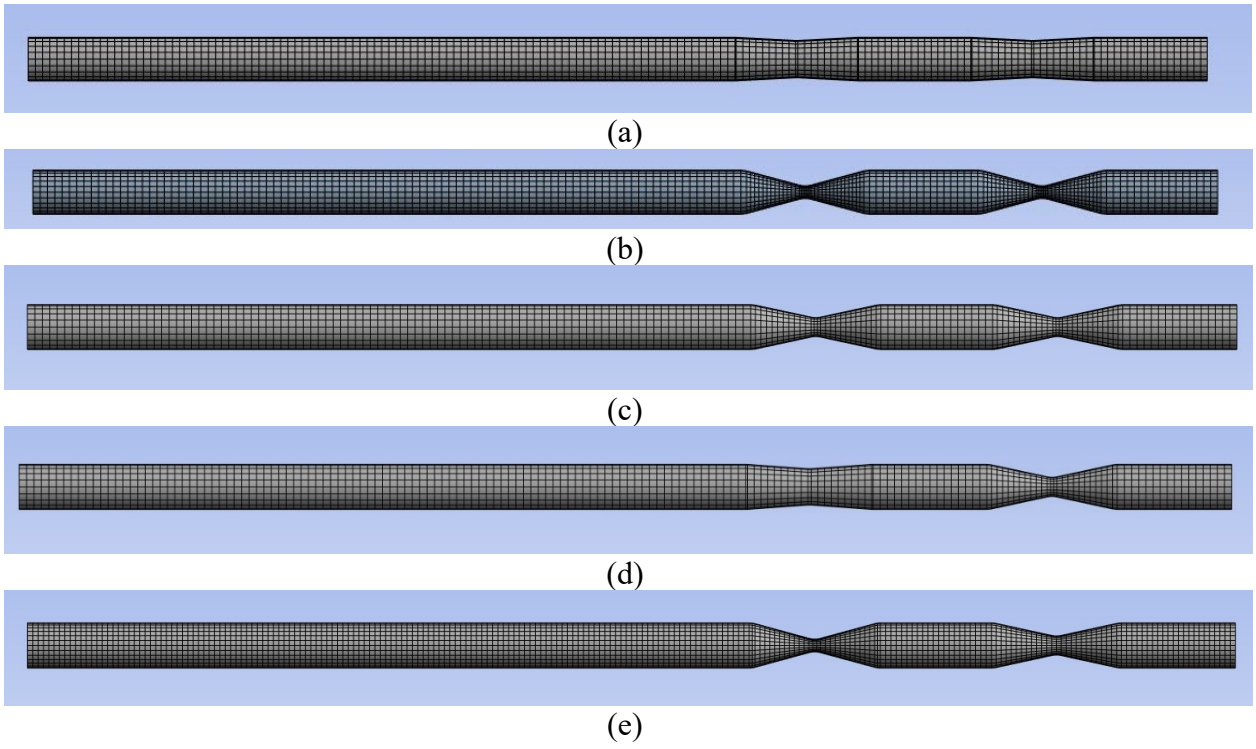

Figure 4: 2D view of structured mesh for (a) 15/15%, (b) 75/75%, (c) 60/60%, (d) 20/60% and (e) 75/60% stenosis

2.3 Problem Formulation

2.3.1 Assumptions

The governing equations, boundary conditions and assumptions made are provided in this section. The Navier-Stokes and continuity equations were used to solve the flow equations. Following the geometry in Figure 1 above, the cylindrical polar coordinates system is used to represent the various points in the domain where r, θ, z denote radial, circumferential and axial

direction respectively. The flow is not dependent on θ because of asymmetrical, hence, θ is neglected.

Below are the assumptions made:

i. The flow is 3-Dimensional, incompressible, and steady.
ii. Blood is Newtonian fluid.
iii. Blood flows as single-phase flow.
iv. Single-phase flow is considered
v. Artery is considered as a rigid wall.
vi. There is no-slip at the solid-fluid interface.
vii. The flow is fully developed.
viii. Gravitational and magnetic forces are neglected.

2.3.2 Governing Equations

The equations that govern are as follows:

Navier-Stokes equation (Mathieu and Scoot, 2000)

$$\frac{\partial u_i}{\partial x_i^2} = 0 \tag{1}$$

$$\frac{\partial u_i}{\partial t} + u_j \frac{\partial u_i}{\partial x_j} = \frac{-1}{\rho}\left(\frac{\partial P}{\partial x_i}\right) + \nu \frac{\partial^2 u_i}{\partial x_j \partial x_i} \tag{2}$$

The Standard *k -ω* Turbulence Model (Hoffmann and Chiang. 2000) was used.

The instantaneous component variables are also given by:

$$u = \overline{u} + u', v = \overline{v} + v', w = \overline{w} + w', P = \overline{P} + P' \tag{3}$$

To further simplify the Navier Stokes equations Eqn. 1 and Eqn. 2, the time average is taken using the instantaneous component variables in Eqn. 3.1 and Eqn. 3.2. A modified Navier-Stokes equation is obtained. This modified equation is called Reynolds Averaged Navier Stokes (RANS) equations. These equations are given below:

$$\frac{\partial}{\partial x_i}(\rho) + \frac{\partial}{\partial x_i}(\rho u_i) = 0 \tag{4}$$

$$\frac{\partial}{\partial t}(\rho u_i) + \frac{\partial}{\partial x_j}(\rho u_i u_j) = \frac{-\partial P}{\partial x_i} + \frac{\partial}{\partial x_j}(2\mu S_{ij}) \tag{5}$$

Where, ρ denotes density of blood, μ represents dynamic viscosity, P represents pressure and S_{ij} denotes Strain-rate tensor.

S_{ij} equation is represented by

$$S_{ij} = \frac{1}{2}\left(\frac{\partial u_i}{\partial x_j} + \frac{\partial u_i}{\partial x_i}\right) \tag{6}$$

Introducing the low *Re k-ω* turbulent model equations to the equations above, the eddy viscosity which came about by flow changes from laminar flow to turbulent flow, is solved. These equations are given by

$$k - equation: \frac{\partial}{\partial t}(\rho k) + \frac{\partial}{\partial x_i}(\rho k u_i) = \frac{\partial}{\partial x_j}(\Gamma_k \frac{\partial k}{\partial x_j}) + G_k - Y_k \tag{7}$$

$$\omega - equation: \frac{\partial}{\partial t}(\rho\omega) + \frac{\partial}{\partial x_i}(\rho\omega u_i) = \frac{\partial}{\partial x_j}(\Gamma_\omega \frac{\partial \omega}{\partial x_j}) + G_\omega - Y_\omega \quad (8)$$

Where, *k* represents turbulence kinetic energy, *ω* denotes specific dissipation rate, $\Gamma_k \Lambda \Gamma_\omega$ represents effective diffusivity, G_k , G_ω are generation terms and Y_k , Y_ω are destruction term.

$$\Gamma_k = \mu + \alpha * \left(\rho \frac{k}{\omega}\right) \frac{1}{\sigma_k} \quad (9)$$

$$\Gamma_\omega = \mu + \alpha * \left(\rho \frac{k}{\omega}\right) \frac{1}{\sigma_\omega} \quad (10)$$

The standard and translational variant *k-ω* turbulence is dependent on Reynolds number which are determined by:

$$\alpha^* = \alpha_\infty * \left(\frac{\alpha_0 * + \frac{R_t}{R_k}}{1 + \frac{R_t}{R_k}} \right) \quad (11)$$

$$G_k = -\rho \overline{u_i} \overline{u_j} \frac{\partial u_j}{\partial x_i} \quad (12)$$

$$G_\omega = \alpha \left(\frac{\omega}{k}\right) G_k \quad (13)$$

$$\alpha = \frac{\alpha_0}{\alpha^*} \left(\frac{\alpha_0 + \frac{R_t}{R_\omega}}{1 + \frac{R_t}{R_\omega}} \right) \quad (14)$$

$$Y_k = \rho\beta * f_{\beta *} k\omega \quad (15)$$

$$\beta_i^* = \beta_\infty * \left(\frac{0.2666 + \left(\frac{\mathrm{Re}_t}{R_\beta}\right)^4}{1 + \left(\frac{\mathrm{Re}_t}{R_\beta}\right)^4} \right) \quad (16)$$

The closure coefficients for translational k-ω model

$\alpha_\infty^* = 1, \alpha_\infty = 0.51, \alpha_0 = 0.1111, \beta_\infty^* = 0.085, \beta_i = 0.071, R_\beta = 7.8, R_k = 5.8,$

$R_w = 2.94, \xi^* = 1.45, M_{t0} = 0.245, \sigma_k = 2.0, \sigma_w = 2$

Lastly, the Reynolds number and velocity are given by:

$$R = \frac{\rho v_{avg} D}{\mu} \quad (17)$$

$$v_{\max} = 2 v_{avg} \quad (18)$$

2.3.3 Boundary Conditions

The boundary conditions used for the 3D model are given below:

(i). **Inlet**: The Poiseuille flow, parabolic velocity profile was used at the inlet for simulation of steady flow.

(ii). **Outlet**: A traction free (zero pressure) condition was used at the outlet of the artery.

(iii). **Wall**: A non-slip condition was considered for the arterial wall.
Table 2 shows the different locations and their boundary conditions

Table 2: Table of boundary conditions

Location	Condition
Wall At $r = R(z)$	$v_r = v_z = 0$ (No slip)
Wall At $r = 0$, $Vz = 0$	$\frac{\partial v_z}{\partial z} = 0$
Inlet at $z = 0$, $Vr = 0$	$v_z = v_{\max}\left(1 - \frac{x^2 + y^2}{r^2}\right)$
Outlet At $z = L$	$\frac{\partial v_r}{\partial z} = \frac{\partial v_z}{\partial z} = 0$
Attached flow $v_z = 0$	$\left(\frac{\partial v_z}{\partial z}\right)_{z=0} > 0\,,\ \frac{\partial p}{\partial z} < 0$
On the verge of separation $v_z = 0$	$\left(\frac{\partial v_z}{\partial z}\right)_{z=0} = 0\,,\ \frac{\partial p}{\partial z} > 0$
Separated flow $v_z > 0$	$\left(\frac{\partial v_z}{\partial z}\right)_{z=0} < 0\,,\ \frac{\partial p}{\partial z} > 0$

2.3.4 Material Properties

The properties of the material are given below in Table 3:

Table 3: Table of material properties (Fetuga *et al*., 2022)

Properties	ρ (kg/m^3)	μ (kg.m/s)
Blood	1050	0.003675
Arterial wall	1095	

3.0 NUMERICAL DESCRETIZATION

The boundary conditions, the continuity and Navier Stokes equations were solved using the ANSYS Fluent CFD software. The discretization scheme was set as Gauss cell based for gradient, second order for pressure, and second order upwind for momentum. In addition, a turbulence model of low-Reynolds number SST *k-ω* model was implemented and 1×10^{-7} convergence criteria were set for all the equations.

4.0 GRID INDEPENDENCE TEST

A grid independence test was carried out on carried out on a 75/75% double stenotic artery with *Re* = 500. The importance of this is to effectively manage the number of grids to save computational time and cost. Five mesh sizes were considered and are presented in ascending order in table 4 below.
The axial velocity at different mesh sizes were compared. From the results, upon further refinement of mesh from Grid 4, there was a constant axial velocity when rounding up to 4 decimal places. Therefore, for the purpose of this project, Grid 4 with element size 82287 and node size of 17825 will be used for this computational study.

Table 4: Grid Independence Test

AXIAL VELOCITY (m/s)			
MESH	**NODES**	**ELEMENTS**	**S = 75/75%**
MESH 1	10258	45631	4.498211
MESH 2	10266	45673	4.485441
MESH 3	10393	46150	4.494524
MESH 4	17825	82287	4.492022
MESH 5	263578	253188	4.492021

4.1 Validation

To validate the models, the axial velocity was studied and compared with experimental work carried out by Ahmed and Giddens (1983) and numerical studies by Kabir *et al.* (2021) literature for a case of 75/75% stenosis at Reynolds number of 500 at axial location of Z=2D and Z=2.5D. The relative axial velocity and relative error are presented in Table 5 below. From the table, at an axial location of Z=2D, the relative axial velocity of this study varied from the study conducted by Kabir *et al.* (2021) by 7.7% and from Ahmed and Giddens (1983) by . Also, at an axial location of Z=2.5D, the relative axial velocity varied by 6.3%. This is within acceptable limits; therefore, this similarity shows the consistency of this numerical model.

Table 5: Validation of numerical model

Model	v_z / v_{avg} at Z=2D	% Error	v_z / v_{avg} at Z=2.5D	%Error
Kabir *et al.*, 2021	0.7429	7.7%	0.9143	6.3%
Ahmed and Giddens	0.975	29.7%	0.95	9.8%
Present work	0.6857	-	0.8571	-

4.1.1 Flow Streamlines

The velocity profile for various Reynolds numbers and at a 75/75% stenosis level were studied. From the results given in Figure 5(a), (b), (c) and (d) below, as blood enters the artery, the velocity begins to increase from the upstream of the proximal stenotic area towards the throat of the stenosis. At the throat of the proximal stenosis, the velocity reaches its peak and then begins to reduce towards the first downstream of the stenotic area. After the first downstream, a repeat of the flow streamline occurs. Blood velocity begins to increase towards the distal stenosis and at the throat, the velocity reaches its peak and begins to decrease towards the second downstream. Because of this difference in velocity, there is an increase in pressure that leads to a separation in the flow. The separated flow is then re-attached at a point further away from the distal stenotic area. This is in much similarity with the numerical study carried out by Fetuga *et al.* (2022) and Kabir *et al.* (2021). This same flow streamline is observed in the Wall Shear Stress contours and is shown in Figure 6(a), (b), (c), (d) and (e).

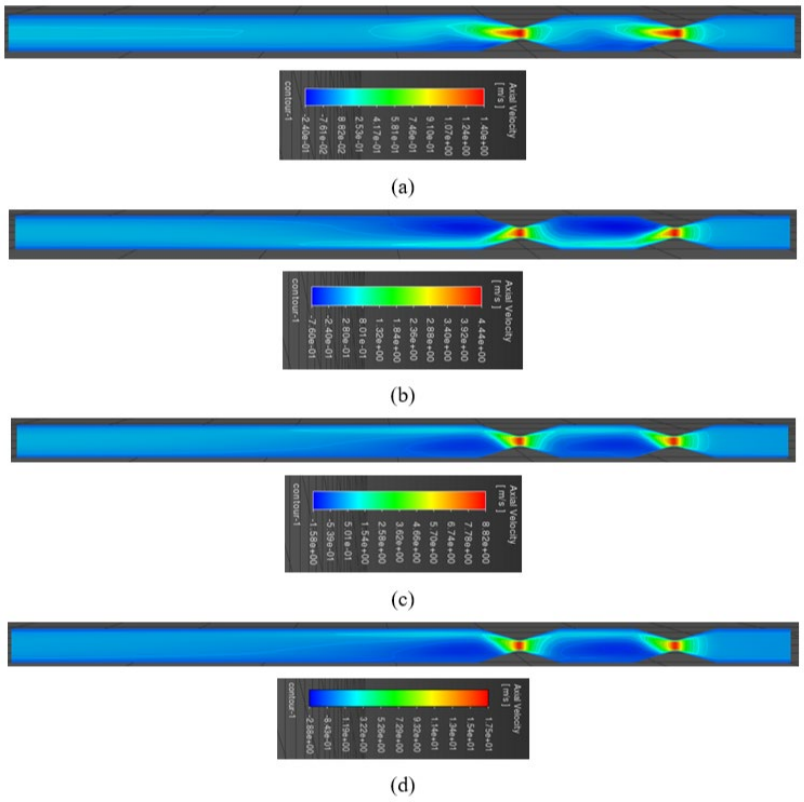

Figure 5: Velocity profile for 75-75% stenosis at (a) Re = 150, (b) Re = 500, (c) Re = 1000, (d) Re = 2000.

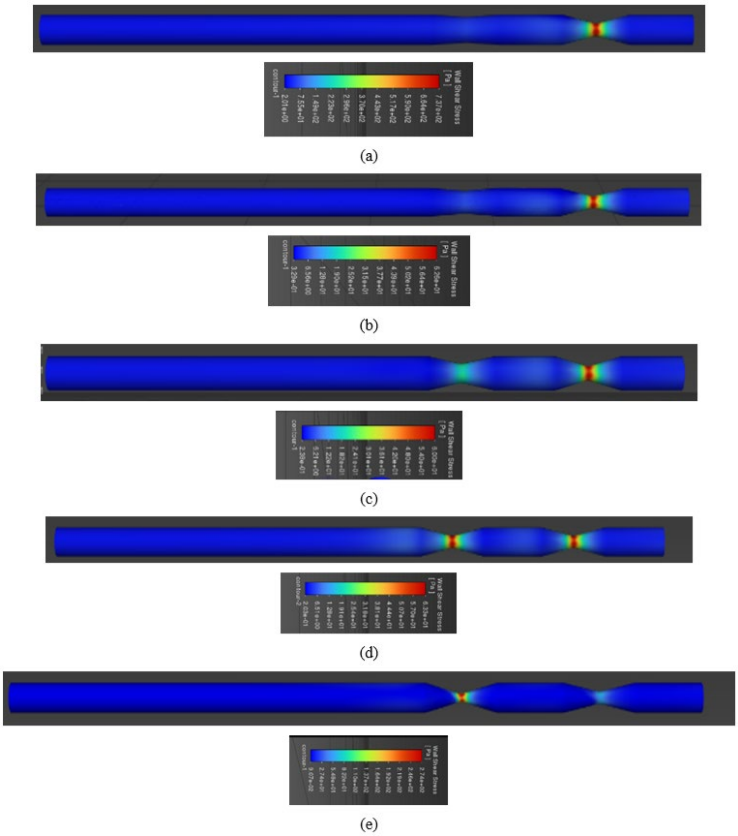

Figure 6: WSS contours at Re = 500 for various levels of (a) 15/60%, (b) 20/60%, (c) 45/60%, (d) 60/60%..., (e) 75/60% ... stenosis

4.2 Effects of Reynolds Number on Axial Velocity

4.2.1 Effects of Reynolds Number on Axial Velocity For 20/60%, 45/60%, 60/60% and 75/60%

The effects of Reynolds number on axial velocity of varying levels of stenosis was studied. Figure 7 below shows the effects of Reynolds number on axial velocity of varying levels of distal stenosis. For a 20/60%, at Reynolds number of 150, a minimum axial velocity of 0.65203 m/s was observed and a maximum axial velocity of 11. 561 m/s was observed. This was very similar to the values obtained for 45/60% stenosis where the minimum and maximum axial velocities were 0.65116 m/s and 11.411 m/s respectively. However, for a 75/60% stenosis, a significant increase was observed with its maximum axial velocity reaching up to 25.471 m/s and a minimum axial velocity of 1.4514 m/s. This shows that at higher levels of distal stenosis, there is a significant increase in velocity due to a greater constriction. In the arteries, when axial velocity increases, it is associated with increased shear stress on the endothelial cells lining the coronary arteries. Increased velocity could also lead to a plaque rupture. Plaque rupture can result in the formation of a blood clot, which can partially or completely block the coronary artery and lead to a heart attack medically known as myocardial infarction. Furthermore, increased blood velocity can elevate the oxygen demand of the heart. If the coronary arteries cannot supply sufficient blood to meet this demand, it can result in ischemia and cause chest pain, known as angina.

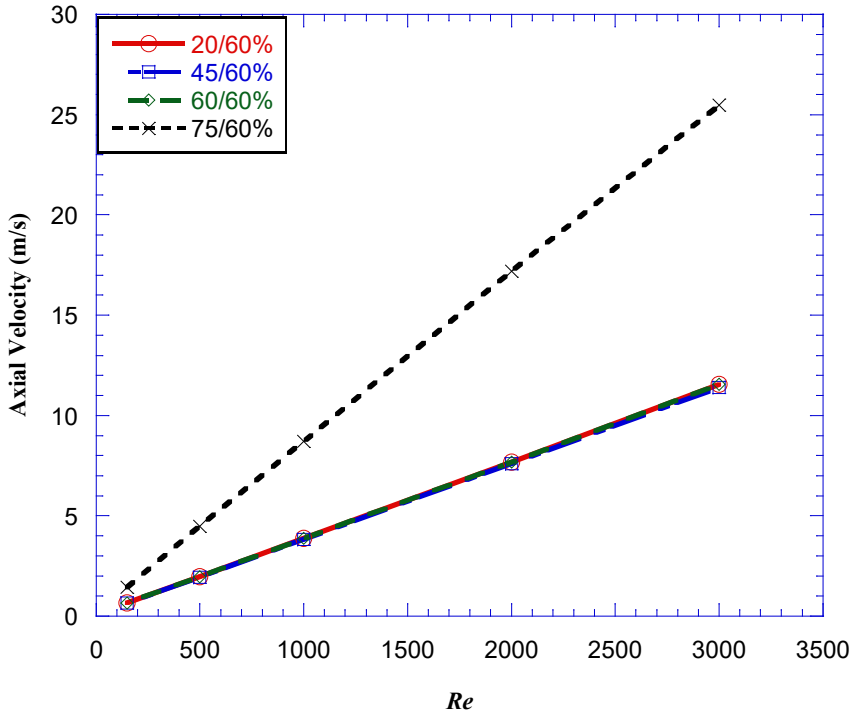

Figure 7: Graph of axial velocity against Re for 20/60%, 45/60%, 60/60% and 75/60% stenosis

4.2.2 Effects of Reynolds Number On Axial Velocity For 15-75% And 75-15%

The effects of Reynolds number on a 15/75% and a 75/15% stenosis was also studied. As seen from Figure 8 below, a similar axial velocity variance was observed. For a 15/75% stenosis, a minimum axial velocity of 1.3818 m/s was observed with a maximum axial velocity of 25.528 m/s. For a 75/15% stenosis, minimum and maximum axial velocities of 1.4168 m/s and 26.003 m/s respectively were recorded. In addition to the effects of axial velocity discussed in

section 4.2.1 above, research has shown that persistent high blood velocity can lead to hypertension. Over time, hypertension can lead to heart failure or death.

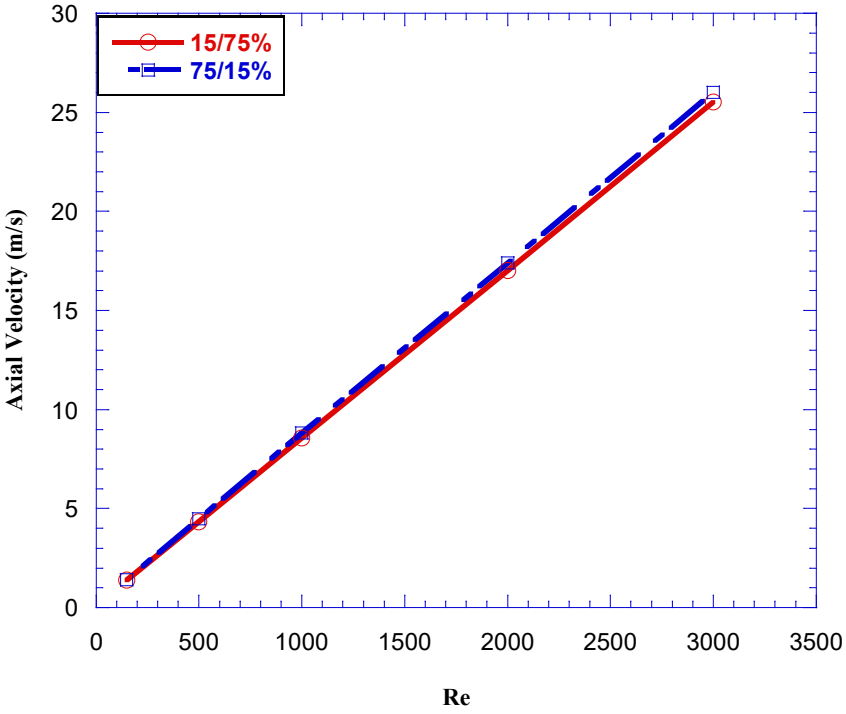

Figure 8: Graph of axial velocity against Reynolds number for 15/75% and 75/15% stenosis

4.3 Effects of Varying Level of Stenosis on Wall Stress

4.3.1 Effects of Varying Level of Distal Stenosis On Wall Shear Stress

Figure 9 shows the comparison of maximum wall shear stress with various levels of distal stenosis while the proximal stenosis is kept constant. From the graph, it can be observed that for all cases of Reynolds number, between 15-60% and 60-60% level of distal stenosis, wall shear stress remains constant. As the level of distal stenosis increases between 60-60% and 75-60%, wall shear stress increases exponentially with 75% level of distal stenosis having the highest Wall shear stress value of 3500 Pa. The lowest Wall shear stress was recorded at 15% level of distal stenosis with a value of 14 Pa. It can also be observed that very little change is recorded between Reynolds numbers of 150 and 500. This is since flow is purely laminar within this region. As Reynolds number increases beyond *Re*=500, there is a significant change in Wall Shear Stress. Hence, it can be inferred that Wall Shear Stress increases with an increasing level of distal stenosis. It is noteworthy that high wall shear stress is associated with formation of vulnerable plaque phenotype and promotes plaque development. High WSS is also associated with damage to the endothelial cells lining the arteries. This damage can lead to endothelial dysfunction, reducing the artery's ability to regulate blood flow and pressure effectively. An excessive WSS also leads to high blood pressure which can in turn leads to heart attack or even death of the individual.

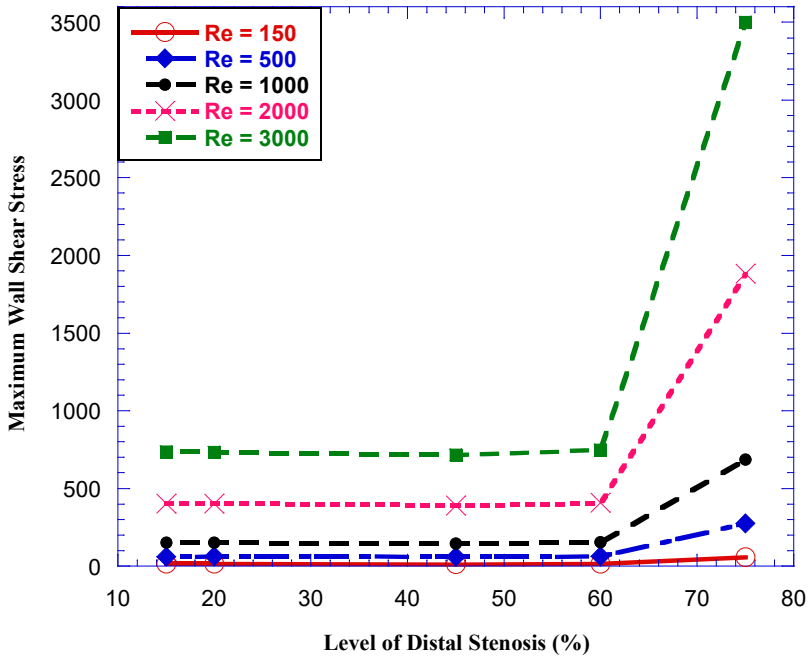

Figure 9: Graph of maximum wall shear stress against percentage level of stenosis

4.3.2 Effects of Varying Level of Proximal Stenosis on Wall Shear Stress

Figure 10 also shows the comparison of maximum wall shear stress with varying level of proximal stenosis i.e., keeping the distal stenosis constant at 60% and varying the proximal stenosis between 15 and 75%. It is evident from the graph that for all cases of Reynolds numbers, maximum wall shear stress remains constant between 15 and 45% levels of proximal stenosis. At 75% stenosis and *Re*=3000, the wall shear stress reaches the peak of 3004 Pa. As previously stated, an excessive WSS also leads to high blood pressure which can in turn leads to heart attack or even death of the individual.

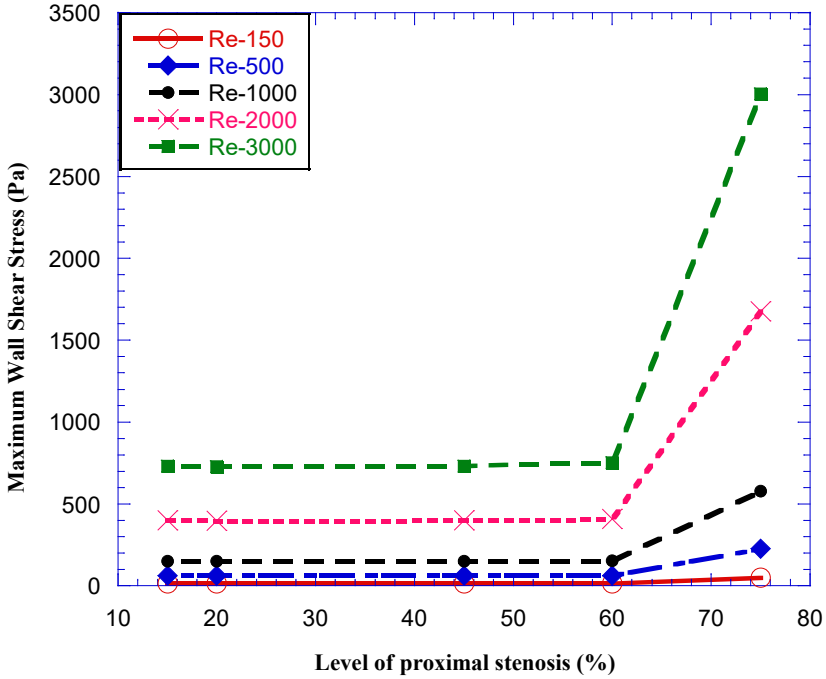

Figure 10: Graph of Maximum wall shear stress against percentage level of stenosis

4.4 Effects of Varying Reynolds Number on Wall Shear Stress

Furthermore, the comparison between wall shear stress and Reynolds number was analyzed. This was conducted on four geometries: 60-15%, 60-20%,60-45%,70-75%. For stenosis levels of 60-15 to 60-45%, the WSS was almost equal for 60-15% to 60-45% and increased gradually with the minimum values at an average of 15 Pa and maximum values at an average of 731 Pa. For a stenosis level of 60-75%, significant changes were recorded . minimum and maximum values of 52 Pa and 3004 Pa respectively. This shows that higher levels of stenosis, there is a drastic increase in WSS as Reynolds number increases. This is line with the research carried out by Kabir *et al.*, 2021. This is shown in Figures 11 (a), (b), (c), (d) and (e).
These results have shown that as Reynolds number increases, indicating higher blood velocity, WSS increases. Extremely high WSS can damage the endothelial cells lining the arteries. This can lead to endothelial dysfunction and further cause more plaque formation.

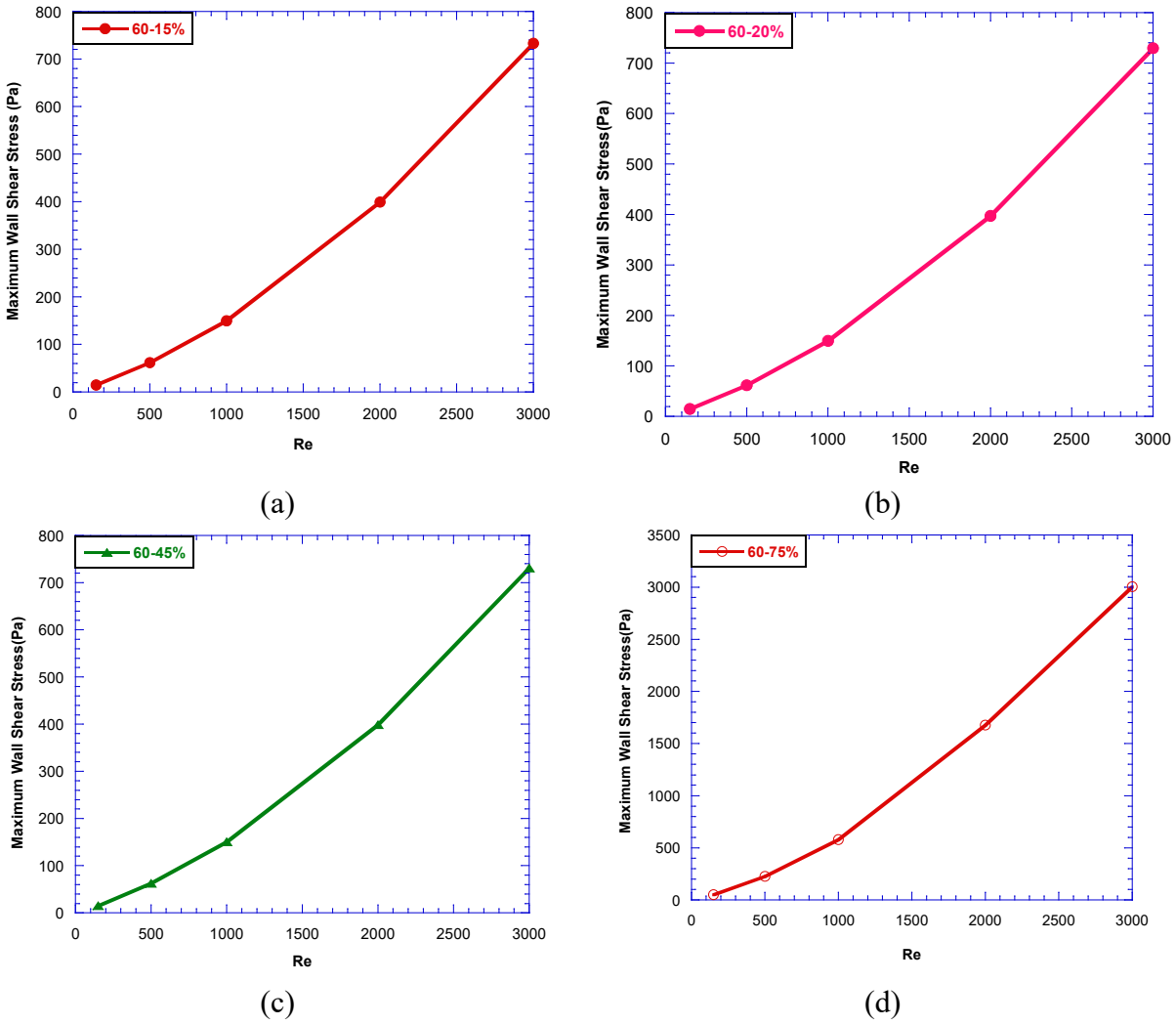

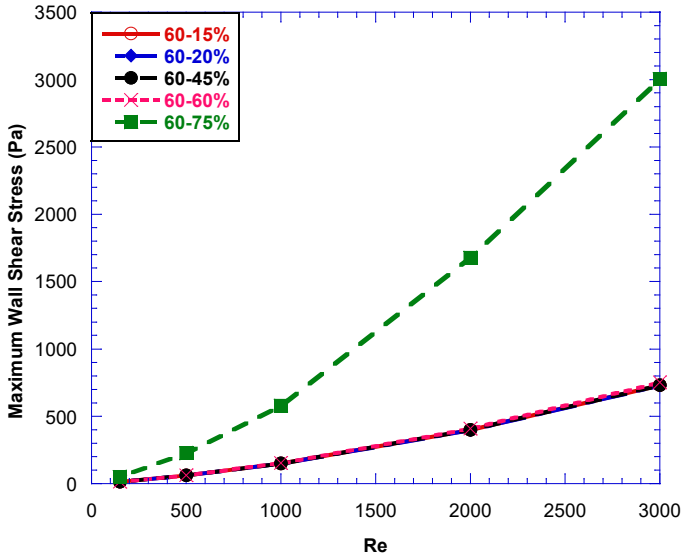

(e)

Figure 4: Graph of Maximum wall shear stress against Reynolds number. for (a) 60-15%, (b) 60-20%, (c) 60-45%, (d)60-60%, (e) 60-75% level of proximal stenosis

4.5 Effects of Reynolds Number on Both Proximal and Distal Recirculation Zone Length

The effects of Reynolds no. on recirculation zone length were studied for 15-60% and 20-60% stenosis and the results are presented in Figure 12(a) and (b) respectively. The graphs show that as Reynolds number increases, dimensionless recirculation zone length decreases but this occurs for only the proximal stenotic site. It can be seen in Figure 12(a) that at 0<*Re*<500, the longest recirculation length is recorded with a peak value of 3.5786D. Between 500<*Re*<2000, recirculation length decreases with a minimum value of 0.8244D. For *Re*>2000, the proximal recirculation zone length remains relatively constant at a value of 0.8D.

Compared with the distal recirculation zone length, Figure 12(a) below shows that recirculation zone length remains constant for 0<Re<3000 and has a value of almost zero indicating that there is no significant recirculation zone at second downstream. The same applies for 20-60% stenosis as shown in Figure 12(b) which had a peak proximal recirculation length of 3.2757D at Re=150 and a minimum proximal recirculation length of 0.8438D at Re=3000.

The findings suggest that at low velocities, the flow separates more easily after the stenosis, thereby creating a longer recirculation zone. As Reynolds no. increases, the inertial forces overpower the viscous forces, which in turn helps in reattaching the flow faster after separation, thus leading to a reduced recirculation length. The negligible recirculation length distal to the second stenosis indicates that blood flow stabilizes fast after the second stenosis due to interaction between the two stenoses. The physiological effect of the prolonged recirculation zone is that it can create a conducive condition for further development of plaques due to the prolonged exposure of the endothelial cells to low and oscillatory shear stress. Oscillatory shear stresses can lead to plaque rupture. If blood clots form in the coronary artery, it can lead to blockage of blood to the heart and then lead to a heart attack.

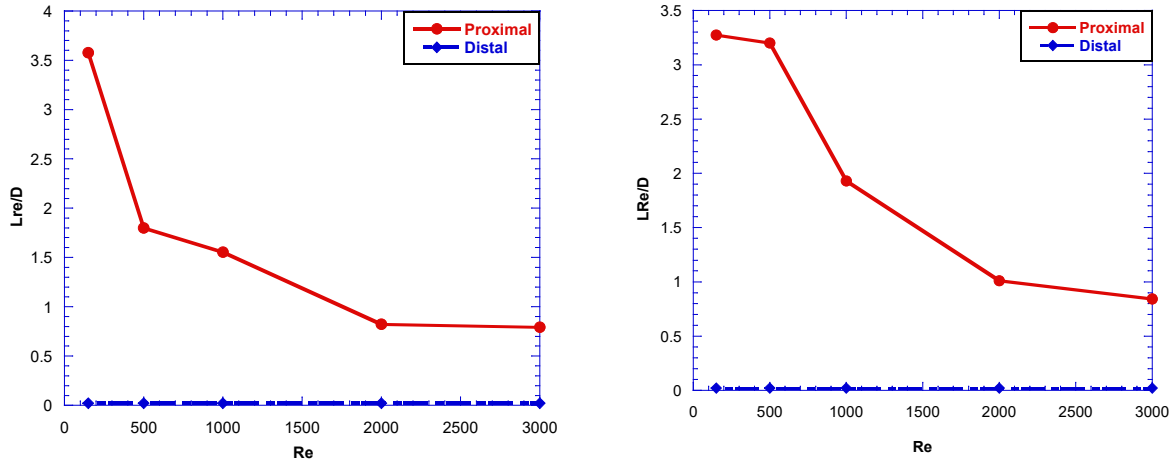

(a) (b)

Figure 5: Graph of dimensionless recirculation zone length against Reynolds number. for (a) 15/60% and (b) 20/60% level of stenosis

4.6 Comparison of Effects of Recirculation Zone Length on Varying Level of Distal and Proximal Stenosis

Figure 13(a) below illustrates the relationship between recirculation and *Re* for varying levels of distal stenosis. From the graph, it can be observed that for all levels of stenosis, as Reynolds number increases, recirculation zone length decreases, this is noticeable in lower levels of stenosis between 15/60% and 45/60%. However, it can be observed that for higher levels of stenosis i.e, 60/60% and 75/60%, the recirculation zone length remains relatively constant. This may indicate persistent flow disturbances that do not significantly change as Reynolds number increases. Furthermore, recirculation zone length remains constant at higher levels of stenosis because the severe reduction in cross sectional area of the artery creates a significant flow disturbance, thereby leading to immediate separation and stable recirculation patterns. The flow disturbance is so pronounced as such that it overrides the influence of other factors that can change the recirculation zone length i.e, a further increase in the Reynolds number will not cause any significant change in the recirculation zone length. As a result, even as Reynolds number increases, the recirculation zone length, the RZL remains relatively constant. This shows a saturation effect where the stenosis itself dictates the flow behaviour. The same applies for varying levels of proximal stenosis shown in Figure 13(b), only that the recirculation zones form earlier and remain relatively constant.

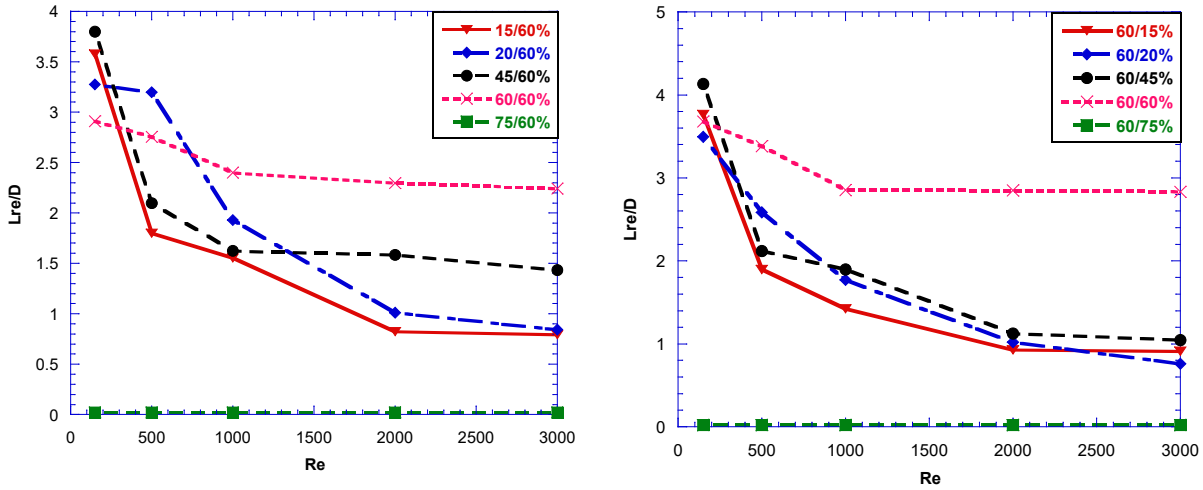

(a) (b)

Figure 6: Comparison of effect of recirculation zone length on varying level of (a) distal and (b) proximal stenosis

5.0 CONCLUSION

A computational fluid dynamics study was conducted to investigate the effects of double stenosis on heamodynamic indicators such as recirculation zone length and wall shear stress in double stenotic arteries of various levels. The simulation was carried out on 11 geometries – 15/60%, 20/60%, 45/60%, 75/60%, 60/15%, 60/20%, 60/45%, 60/60%, 60/75%, 15/75%, 75/15%, using ANSYS FLUENT. Five Reynolds numbers were considered – *Re* = 150, 500, 1000, 2000, 3000 and the major findings in this research are:

(i) At low Reynolds number, recirculation zone length is high while it is lower at higher Reynolds number, i.e., as Reynolds number increases, recirculation zone length decreases.

(ii) When varying both distal and proximal stenosis, as Reynolds number increases, recirculation zone length decreases in lower levels of stenosis between 15/60% and 45/60% while it remains relatively constant for higher levels of stenosis i.e., 60/60% and 75/60%.

(iii) As Reynolds number increases, maximum wall shear stress increases.

(iv) When varying both distal and proximal stenosis, as Reynolds number increases, maximum wall shear stress increases gradually at lower levels of stenosis with almost equal values. At higher levels of stenosis, there was rapid increase in maximum wall shear stress as Reynolds number increases.

(v) The velocity flow streamlines and the WSS contours were also presented.

This study assumed that blood was a Newtonian fluid for simplicity of computation. However, blood is a non-Newtonian fluid. Using a non-Newtonian model such as Casson model could influence wall shear stress distributions and flow streamlines. Future studies should incorporate non-Newtonian behaviours to get a more accurate representation.

REFERENCES

Alshare, A., Bourhan, T., Hossam H. E. (2013). Computational Modeling of Non-Newtonian Blood Flow Through Stenosed Arteries in the Presence of Magnetic Field. [DOI: 10.1115/1.4025107].

Alshare, A., Tashtoush, B. (2015). Simulations of Magnetohemodynamics in Stenosed Arteries in Diabetic or Anemic Models. Computational and Mathematical Methods in Medicine Volume 2016, Article ID 8123930, 13 pages http://dx.doi.org/10.1155/2016/8123930.

Changdar, S.,and De, S. (2015). Numerical Simulation of Nonlinear Pulsatile Newtonian Blood Flow through a Multiple Stenosed Artery. Hindawi Publishing Corporation International Scholarly Research Notices Volume 2015, Article ID 628605, 10 pages http://dx.doi.org/10.1155/2015/62860

Daniel, J. T., Jeroen, F., Krzysztof, C., Ian, H., D.R., Hose, Rebecca, G., Louise, A. , Marcel, v. V., Danielle, C. J. K.,

Pim, T., Michel, R., Julian P. G., and Paul D. M. (2023). Validation of a novel numerical model to predict regionalized blood flow in the coronary arteries. European Heart Journal - Digital Health (2023) 4, 81–89 https://doi.org/10.1093/ehjdh/ztac077

Dattani, S., Samborska, V., Ritchie, H. Roser, M. (2021). Cardiovascular Diseases. https://ourworldindata.org/cardiovasculardiseases.

Doutel E., Carneiro J., Campos J.B.L.M., Miranda J. M. (2018). Artificial stenoses for computational hemodynamics

Dwidmuthe, P. D., Dastane, G. G., Mathpati, C. S., Joshi, J. B., Changdar, S., De, S. (2015). Study of Blood Flow in Stenosed Artery Model Using Computational Fluid Dynamics and Response Surface Methodology. doi: 10.1002/cjce.23991

Editors at Mount Sinai. (2024). Hardening of the arteries. https://www.mountsinai.org/health-library/disease-conditions/hardening-of-the-arteries

Editors at RWJ Barnabas Health. Heart, Vascular and Thoracic Diseases and Conditions. https://www.rwjbh.org/treatment-care/heart-and-vascular- care/diseases-conditions/renal-artery-stenosis/

Editors at Vascular Interventional Radiology Clinic. (2011) https://virclinic.com/stroke/carotid-arterystenosis/

Fetuga, I. A., Olakoyejo, O.T., Oluwatusin, O., Adelaja, A. O., Gbegudu, J. K., Aderemi, K. S., Adeyemi, E. A., (2023). Computational Model of Nano-Pharmacological Particles for the Clinical Management of Stenotic and Aneurysmatic Coronary Artery in the Human Body. Nigerian Journal of Technological Development, Vol. 20, No. 1, March 2023. Online ISSN: 2437-2110.

Fetuga, I.A., Olakoyejo, O.T., Ewim, D. R. E., Oluwatusin, O., Adelaja A. O., Aderemi K.S. (2022). Numerical prediction of flow recirculation length zone in an artery with multiple stenoses at low and high Reynolds number. Series on Biomechanics, Vol.36 No.4 (2022), 10-24. DOI:10.7546/SB.03.04.2022

Hoffmann, K. A., and Chiang, S. T., Computational Fluid Dynamics Volume III, 4th Ed., EES, Wichita, KS, USA, 2000.

Hussain, A., Dar, M. N. R., Cheema, W. K., Tag-eldin, E. M., Kanwal, R. (2023). Numerical Simulation of Unsteady Generic Newtonian Blood Flow and Heat Transfer Through Discrepant Shaped Dilatable

Kabir A., Alam F., Uddin A., (2021). Numerical simulation of pulsatile blood flow: a study with normal artery, and arteries with single and multiple stenosis. Journal of Engineering and Applied Science (2021) 68:24. https://doi.org/10.1186/s44147-021-00025-9 .

Kabir, A., Alam F and Uddin A. (2018). A Numerical Study on the Effects of Reynolds Number on Blood Flow with Spiral Velocity Through Regular Arterial Stenosis Chiang Mai J. Sci. 2018; 45(6): 2515-2527 http://epg.science.cmu.ac.th/ejournal/

Kamanagar, S. (2021). Numerical simulation of pulsatile blood flow characteristics in multi stenosed coronary artery. Bio-Medical Materials and Engineering 1 (2021) 1–13 1 DOI 10.3233/BME-211234.

Koosha, N., Mosavi, V., Kheirollah, J., Najafi, N., Alizadeh, A., Ranjbari, L., Aminian, S. (2023). Numerical Simulation of Effect of Hybrid Nanofluid on Heat Transfer and Flow of the Newtonian Pulsatile Blood Through 3D Occluded Artery: Silver and Gold Nanoparticles. Journal of Thermal Biology 117 (2023) 103718. https://doi.org/10.1016/j.jtherbio.2023.103718.

Mamun, K., Akhter, M. N., Funazaki, K. (2018). Simulation of Physiological Non-Newtonian Blood Flow through 3-D Geometry of Carotid Artery with Stenosis. IOSR Journal of Mechanical and Civil Engineering (IOSR-JMCE) e-ISSN: 2278-1684,p-ISSN: 2320-334X, Volume 15, Issue 1 Ver. IV (Jan. - Feb. 2018), PP 33-43. DOI: 10.9790/1684-1501043343.

Mathieu, J., and Scoot, J., (2000). An Introduction to Turbulent Flow, 1st ed., Cambridge University Press, Cambridge, UK.

Moawad, A. M. A., Abdel-Wahab, A. M., Mekheimer, K. S., Ali, K. K., Sweed, N. S. (2022). Effects of Electro-osmotic and Double Diffusion on Nano-Blood Flow through Stenosis and Aneurysm of the Subclavian Artery: Numerical Simulation. WAVES IN RANDOM AND COMPLEX MEDIA. DOI: 10.1080/17455030.2022.2100945.

Mojra, A., Tafazzoli-Shadpour, M. and Tafti, E. Y. (2007). Computational Analysis of Asymmetric Arterial Stenosis with Applications of Fluid-Solid Interaction. Biomed 06, IFMBE Proceedings 15, pp. 567-571, 2007.

Nadeem, S., Ali, S., Akkurt, N., Ben Hamida, M. B., Almutairi, S., Ghazwani, H. A., Eldin, S. M., Khan, Z. A., Al-Shafay, A. S. (2023). Modeling and Numerical Simulation of Non-Newtonian Arterial Blood Flow for Mild to Severe Stenosis. Alexander Alexandria Engineering Journal (2023) 72, 195–211. https://doi.org/10.1016/j.aej.2023.03.088.

Shaikh, F., Shaikh, A. A., Hincal, E., Qureshi, S. (2023). Comparative Analysis of Numerical Simulations of Blood Flow Through the Segment of an Artery in the Presence of Stenosis. Journal of Applied Mathematics and Computational Mechanics 2023, 22(2), 49-61. DOI: 10.17512/jamcm.2023.2.05.

Tabe, R., Ghalichi, F., Hossainpour, S., Ghasemzadeh, K. (2020). Laminar-to-Turbulence and Relaminarization Zones Detection by Simulation of Low Reynolds Number Turbulent Blood Flow in Large Stenosed Arteries. Bio-Medical Materials and Engineering 27 (2016) 119–129 119 DOI 10.3233/BME161574.

Taylor, D., Feher, J., Czechowicz, K., Halliday, I., Hose, D.R., Gosling, R., Aubiniere-Robb, L., Veer, M. V. Danielle C.

J. Keulards, Tonino, P., Rochette M., Gunn, J. P., and Morris, P. D. (2022). Validation of a novel numerical model to predict regionalized blood flow in the coronary arteries. European Heart Journal - Digital Health (2023) 4, 81–89 https://doi.org/10.1093/ehjdh/ztac077

Violeta, C., Nelson, R., Rui, A. L, Senhorinha T. (2020). Numerical simulation of blood pulsatile flow in stenotic coronary arteries: The effect of turbulence modeling and non-Newtonian assumptions. 978-1-7281-6503-5/20/$31.00 ©2020 IEEE. DOI 10.1109/CSCC49995.2020.00027

Zhao, Y., Wang, H., Chen, W., Sun, W., Yu, X., Sun, C. (2023). Time-resolved Simulation of Blood Flow Through Left Anterior Descending Coronary Artery: Effect of Varying Extent of Stenosis on Hemodynamics. BMC Cardiovascular Disorders (2023) 23:156 1 - 13 https://doi.org/10.1186/s12872023-03190-2